

This is the accepted manuscript made available via CHORUS. The article has been published as:

Topological crystalline insulators and Dirac octets in antiperovskites

Timothy H. Hsieh, Junwei Liu, and Liang Fu

Phys. Rev. B **90**, 081112 — Published 20 August 2014

DOI: [10.1103/PhysRevB.90.081112](https://doi.org/10.1103/PhysRevB.90.081112)

Topological Crystalline Insulators and Dirac Octets in Anti-perovskites

Timothy H. Hsieh,^{1,*} Junwei Liu,^{1,†} and Liang Fu^{1,‡}

¹*Department of Physics, Massachusetts Institute of Technology, Cambridge, MA 02139*

We predict a new class of topological crystalline insulators (TCI) in the anti-perovskite material family with the chemical formula A_3BX . Here the nontrivial topology arises from band inversion between two $J = 3/2$ quartets, which is described by a generalized Dirac equation for a “Dirac octet”. Our work suggests that anti-perovskites are a promising new venue for exploring the cooperative interplay between band topology, crystal symmetry and electron correlation.

PACS numbers: 71.20.-b

Topological crystalline insulators (TCIs)¹ are new topological phases of matter in two and three dimensions which exhibit metallic boundary states protected by crystal symmetry, unlike Z_2 topological insulators (TIs) that rely on time-reversal symmetry²⁻⁴. The first realization of topological crystalline insulators has recently been predicted⁵ and observed in IV-VI semiconductors SnTe, $Pb_{1-x}Sn_xSe$ and $Pb_{1-x}Sn_xTe$ ⁶⁻⁸. These TCIs exhibit a variety of novel topological electronic properties such as Dirac mass generation via ferroelectric distortion^{9,10} and strain-induced flat band superconductivity¹¹, which are not only of fundamental interest but also may enable novel device applications¹²⁻¹⁶. On the theoretical frontier, the discovery of TCIs has sparked intensive efforts in classifying topological phases in different crystal symmetry classes¹⁷⁻²⁴. Given these developments, there is great interest in finding new TCI materials, especially those outside the family of narrow-gap semiconductors. Recent proposals range from pyrochlore iridates²⁵ and multilayer graphene²⁶ to heavy fermion compounds^{27,28}.

In this work, based on a combination of topological band theory, $k \cdot p$ model and first-principles calculations, we predict a new class of TCIs in the anti-perovskite material family A_3BX , with Sr_3PbO and Ca_3PbO as two representatives. Here A denotes alkaline-earth or rare-earth metals (Ca, Sr, La), B denotes main group elements of the p-block (Pb, Sn), and X denotes non-metals (C, N, O)²⁹. The anti-perovskite structure is based on a perovskite but switches the positions of metal and nonmetal elements, see Fig.1a. Anti-perovskites exhibit a wide range of interesting physical properties, such as superconductivity³⁰, giant magnetoresistance³¹, negative thermal expansion³², and magnetocaloric³³ effect, due to the cooperative interactions among lattice, spin, and charge degrees of freedom. Our prediction of TCIs in anti-perovskites thus opens up a promising new venue for topological phases in correlated electron systems.

Our work builds on recent theoretical calculations^{34,35} that noted an unusual low-energy band structure in Ca_3BiN and Ca_3PbO , in which both the conduction and valence bands at the Γ point are $J = \frac{3}{2}$ multiplets with four-fold degeneracy, which correspond to the d -orbitals of the A atom (Ca) and the p -orbitals of the B atom (Bi or Pb). These two sets of orbitals have opposite parities, leading to two possible band orderings at Γ . The

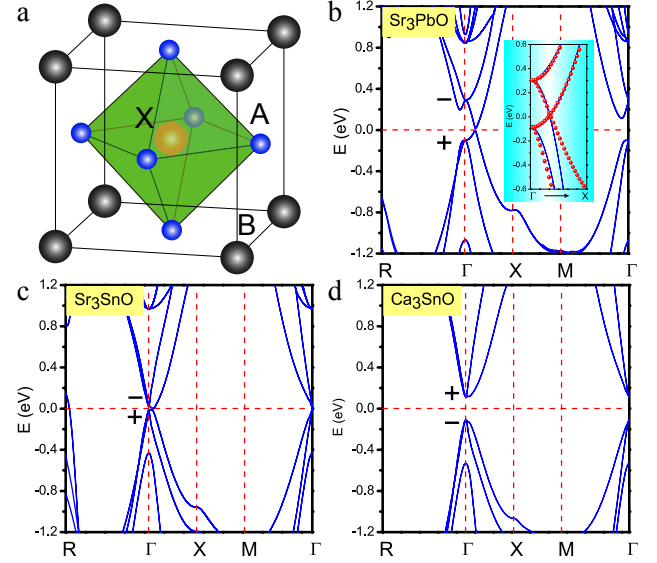


FIG. 1: (a) Crystal structure of the anti-perovskite A_3BX . (b) Band structure of TCI Sr_3PbO in which the orbital character of valence and conduction bands within a Dirac octet is inverted (\pm denote the parities of the band orbitals). The inset depicts a fit with the $k \cdot p$ theory described in the main text. There is a small avoided crossing along ΓX direction. (c) Sr_3SnO is near a topological phase transition with gap closing at Γ . (d) Ca_3SnO is a trivial insulator.

normal ordering corresponds to the d -orbitals of A lying above the p -orbitals of B, which is expected for an ionic insulator (e.g., Ca_3SnO) made of A^{2+} , B^{4-} and O^{2-} , hence topologically trivial. However, Ca_3BiN and Ca_3PbO were found to have an inverted band ordering in which the energies of the d - and p -orbitals are switched. Such a band inversion in anti-perovskites can be induced by decreasing the lattice constant or changing the chemical elements (e.g., $Sn \rightarrow Pb$). However, because of the four-fold degeneracy of the $J = \frac{3}{2}$ multiplet, this band inversion does not change the product of parity eigenvalues of the valence bands. It then follows from the parity criterion³⁶ that anti-perovskites with inverted gaps are *not* topological insulators, as correctly pointed out in Ref.^{34,35}.

Here we show that despite being trivial in the Z_2 clas-

sification of TIs, inverted anti-perovskites are TCIs in the same universality class as SnTe, which are protected by mirror symmetry and indexed by an integer topological invariant known as mirror Chern number³⁷. We find a nonzero mirror Chern number $|n_M| = 1 + 1 = 2$ arises from the aforementioned band inversion between $J = \frac{3}{2}$ quartets in anti-perovskites. Remarkably, near the band inversion transition, the low-energy theory of anti-perovskites at Γ is described by a novel generalization of three-dimensional Dirac fermion to eight-component and spin-3/2, which we term “Dirac octet”.

We first present first-principles calculations of the band structures of three anti-perovskite compounds: Sr_3PbO , Sr_3SnO , and Ca_3SnO , see Fig.1b-d. Our calculations were performed in the framework of density functional theory, by using the Perdew-Burke-Ernzerhof (PBE) generalized gradient approximation³⁸ and the projector augmented wave potential³⁹, as implemented in the Vienna *ab initio* simulation package⁴⁰. The energy cutoff of the plane-wave basis is 400 eV. The $11 \times 11 \times 11$ Monkhorst-Pack k points are used for bulk calculations. Structural relaxations are performed with forces converged to less than 0.001 eV/Å, and spin-orbit coupling is included. To overcome the underestimation of band gap, we employed Heyd-Scuseria-Ernzerhof (HSE) screened Coulomb hybrid density functionals⁴¹ to calculate the bulk electronic structures. By analyzing band parities at Γ as mentioned above, we find that Ca_3SnO and Sr_3PbO belong to the normal and inverted regime respectively, with opposite orderings of d - and p -orbitals, while Sr_3SnO lies very close to the topological phase transition point. Moreover, we find that Ca_3PbO , Ba_3PbO , Ca_3SiO , Ca_3GeO , Ca_3SnO , Ca_3BiN , and Sr_3BiN are also candidate TCIs (see Supplementary Material⁴²).

As a main result of this work, we now reveal the implication of the above band inversion in the context of TCI. For this purpose, we first develop $k \cdot p$ theory for this wide class of anti-perovskites. We find that to linear order in \mathbf{k} , the cubic point group symmetry dictates the following eight-band $k \cdot p$ Hamiltonian describing the $J = \frac{3}{2}$ conduction and valence bands near Γ :

$$H(\mathbf{k}) = m\tau_z + v_1\tau_x\mathbf{k} \cdot \mathbf{J} + v_2\tau_x\mathbf{k} \cdot \tilde{\mathbf{J}} \quad (1)$$

Here τ are Pauli matrices with $\tau_z = \pm 1$ labeling the valence and conduction band orbitals. \mathbf{J} are the spin-3/2 matrices and $\tilde{\mathbf{J}}$ are the only other set of 4 by 4 matrices which transform like the vector \mathbf{k} under the cubic point group⁴². The form of the above $k \cdot p$ Hamiltonian is uniquely determined by requiring invariance under spatial inversion (represented by $P = \tau_z$), time reversal ($\Theta = e^{-i\pi J_y} K$, K being complex conjugation), and discrete rotations of the cubic group O_h generated by \mathbf{J} which act on spin and spatial coordinates simultaneously.

The Hamiltonian (1) can be regarded as a novel generalization of Dirac Hamiltonian in three dimensions, involving an octet of spin-3/2 relativistic fermions that form two four-fold degenerate multiplets at $\mathbf{k} = 0$ protected by the cubic point group symmetries. Moreover,

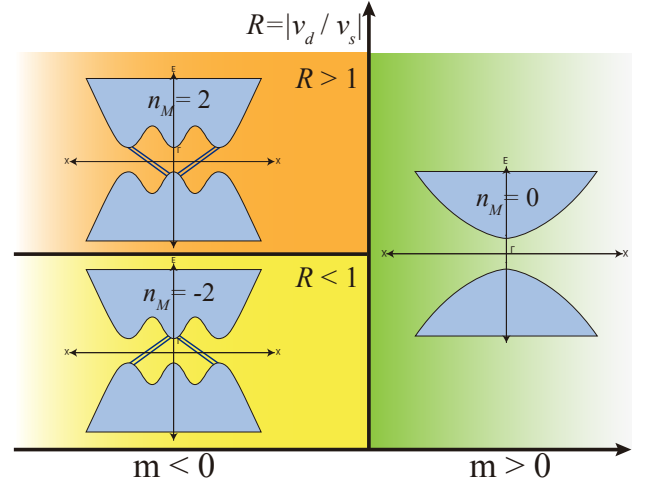


FIG. 2: Topological phase diagram for the minimal quadratic $k \cdot p$ theory describing a Dirac octet, for the (100) mirror plane. The three phases have different mirror Chern number (n_M). Each inset is a schematic band structure depicting bulk states in light blue and surface states in dark blue, cutting through the bulk gap. The existence of the surface states is dictated by n_M .

Eq.(1) involves two velocities, leading to two sets of direction-dependent energy-momentum dispersions. In a special limit to be discussed later, Eq.(1) reduces to two identical copies of Dirac fermions.

We now analyze the mirror Chern number of $H(\mathbf{k})$. There are two sets of symmetry-equivalent mirror planes: (001) and (110). Let us first consider symmetry of reflection with respect to the (100) mirror plane: $x \rightarrow -x$, which is represented by $M = PC_2 = \tau_z e^{-i\pi J_x}$ where C_2 is rotation by π about the x -axis. Note that because $M^2 = -1$, its eigenvalues are $\pm i$. Due to this mirror symmetry, the eight-band Hamiltonian $H(k_x = 0, k_y, k_z)$ commutes with M and thus decouples into two mirror subspaces, with mirror eigenvalue $\pm i$. The four states that span a given mirror subspace are given by the eigenstates of J_x , whose τ_z eigenvalue is locked to j_x eigenvalue. The corresponding four-band Hamiltonian $H_{\pm i}(k_y, k_z)$ within a mirror subspace is given by

$$H_{\pm i}(k_y, k_z) = \mp m(i e^{-i\pi J_x}) + \sum_{i=y,z} k_i (v_1 J_i + v_2 \tilde{J}_i). \quad (2)$$

Remarkably, we find the mirror Chern number n_M depends on not only the sign of m which controls the band inversion at Γ , but also the velocities v_1 and v_2 . We find it convenient to use the linear combinations $v_d \equiv v_1/2 - v_2, v_s \equiv v_1 + v_2/2$ for velocities, and plot the topological phase diagram as a function of m and $R \equiv |v_d/v_s|$ in Fig.2, which consists of three distinct phases with $n_M = 0, 2$ and -2 . To obtain this result, we first consider a special limit $v_s = 0$, for which the four-band Hamiltonian $H_{\pm i}(k_y, k_z)$ reduces to two identical

flavors of two-component Dirac Hamiltonian:

$$H_{\pm i}^{v_s=0}(k_y, k_z) = \mp m\Gamma_0 + v_d(k_y\Gamma_1 - k_z\Gamma_2). \quad (3)$$

where the 4×4 Gamma matrices are found to be $\Gamma_0 \equiv \sigma_z \otimes 1$, $\Gamma_1 \equiv \sigma_x \otimes \sigma_x$ and $\Gamma_2 \equiv \sigma_y \otimes \sigma_x$ (written here in the j_x basis), which forms the $SU(2)$ algebra. When the Dirac mass m changes sign, the Chern number of the $\pm i$ mirror sector changes by ∓ 2 , where the factor of two is due to the flavor degeneracy. Therefore, as m changes from positive to negative, the mirror Chern number changes from $n_M = 0$ to $n_M = 2$. In accordance with convention, we designate $m > 0$ to the trivial phase with normal band ordering as in Ca_3SnO , and $m < 0$ to the TCI phase with inverted band ordering as in Sr_3PbO .

To determine the mirror Chern number for $v_s \neq 0$, we need to account for potential gap closings even when m is fixed to be nonzero. For this, we go beyond linear order in k and simply make the replacement

$$m \rightarrow m + \alpha k^2 \quad (4)$$

where $\alpha > 0$. This is similar to the quadratic term in the BHZ model⁴³. While several $O(k^2)$ terms are allowed by symmetry, we focus on the above for simplicity and find that it qualitatively reproduces the band dispersion from ab initio calculations (Fig.1b), especially in the inverted regime.

To gain intuition for the band dispersion, first consider the limit of zero hybridization between valence and conduction orbitals ($v_s = v_d = 0$). In the trivial regime ($m > 0$), the conduction and valence bands do not cross. However, in the inverted regime ($m < 0$), the bands cross at $\sqrt{|m|/\alpha}$ and restoring the hybridization (v_s, v_d) opens a gap at this crossing.

Importantly, we find that tuning the ratio v_d/v_s closes and reopens this gap along the ΓX directions, with criticality at $v_d/v_s = \pm 1$. To model this gap behavior, we derive the most general $k \cdot p$ theory for this avoided crossing in the Supplementary Material and we state the result here:

$$H_{k_0} = m_0\sigma_z + v_z\delta k_z(\gamma + s_z\sigma_x) + v(k_xs_y - k_ys_x)\sigma_x$$

Here $s_z = \pm 1$ denotes the Kramers pair ($j_z = \pm 3/2$), $\sigma_z = \pm 1$ denote valence and conduction band orbitals, m_0 is the mass term determining the gap, and v and v_z, γ govern the velocities of dispersion in the $x(y), z$ directions. $\delta k_z \equiv k_z - k_0$, where k_0 is the momentum at which the gap is minimum, if $\gamma = 0$. Since there are four such ΓX directions on the $k_x = 0$ mirror plane, every time the four gaps close and reopen (corresponding to m_0 changing sign), the mirror Chern number (of the $k_x = 0$ mirror plane) changes by 4.

Therefore, in going from the previously analyzed limit $|v_d/v_s| = \infty$ to $|v_d/v_s| = 0$, the mirror Chern number changes from $n_M = 2$ to $n_M = -2$ at $|v_d/v_s| = 1$. In the Supplementary Material, we provide a detailed derivation of this. The phase diagram is shown in Fig. 2; we

emphasize that in the inverted regime, the phases are always topologically nontrivial $|n_M| = 2$. Unlike the SnTe class of materials, in which band inversion of spin 1/2 fermions at different points in momentum space add up to yield $|n_M| = 2$, here the band inversion occurs at a single point Γ and it is the spin 3/2 nature of the octet which yields $|n_M| = 2$.

Our theory thus captures and deduces the consequences of two essential features of the band structure of several anti-perovskites: 1) the band inversion of the octet at Γ which as shown above gives rise to 2) a small gap (avoided crossing) at finite momentum along ΓX in such band inverted anti-perovskites. Previous works by Kariyado and Ogata^{35,44} have focused on this finite k avoided crossing at the Fermi energy; they attributed the smallness of the gap (15 meV for Ca_3PbO) to the combination of hybridization with orbital states away from the Fermi energy and spin-orbit coupling. While prior works have emphasized the massive Dirac fermions at finite k near Γ , the main feature of this work is the “parent” Dirac octet at Γ , whose inverted nature gives birth to not only the Dirac fermions at finite k but also the TCI phase.

This nontrivial bulk topological invariant has the following consequences for surface states. Consider any surface which respects reflection symmetry about the (100) or equivalent mirror plane of the crystal. Along the projection of the mirror plane to the surface, there will be two sets of gapless, counter-propagating surface states dictated by the mirror Chern number $n_M = \pm 2$ (see depiction in Fig. 2), similar to the case of SnTe⁵. The locking between mirror eigenvalue and directionality of these surface states depends on the sign of n_M . We note that a previous work by Kariyado and Ogata discovered surface states in a tight-binding model of Ca_3PbO ³⁵, which are closely related to the TCI surface states. However, the tight binding model they used produces a crossing, not avoided crossing, at finite k , and from this bulk gapless phase it is not possible to infer the band connectivity of the surface states or discuss their topological origin. We leave a detailed study of the TCI surface states to future work.

A similar analysis applies to the (1 $\bar{1}$ 0) and symmetry equivalent mirror planes (see Supplementary Material for derivation⁴²), and we summarize the result here and in the phase diagram of Fig. 3: unlike the (100) plane, the (1 $\bar{1}$ 0) has both trivial ($|n_M| = 0$) and nontrivial ($|n_M| = 2$) phases in the inverted regime ($m < 0$). Hence, we introduce the notation (n_{M1}, n_{M2}) to capture the potentially different mirror Chern numbers of the (100) and (1 $\bar{1}$ 0) planes. To fully determine these topological quantum numbers for each inverted anti-perovskite compound requires a careful analysis of first-principle results, which is left to future work.

The above theory applies to many anti-perovskite materials such as Ca_3PbO and Sr_3PbO and captures both essential features of the band structure—an inverted octet at Γ which gives rise to an avoided crossing at finite k . As

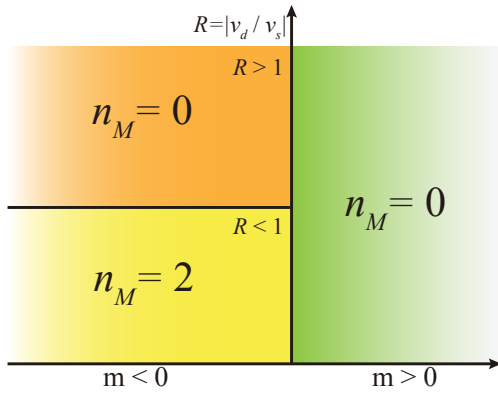


FIG. 3: Topological phase diagram for the minimal quadratic $k \cdot p$ theory of $(1\bar{1}0)$ mirror plane. The numbers n_M are the mirror Chern number.

a result, we have demonstrated the existence of topological crystalline insulators in the anti-perovskite material class, with Ca_3PbO and Sr_3PbO as representative examples with mirror Chern number $|n_M = 2|$ on the (100) and symmetry related mirror planes.

The experimental feasibility of thin film and heterostructure growth, strain, and alloying may add to the already diverse features of this material class. As thin films of SnTe are examples of two-dimensional topological crystalline insulators protected by mirror symmetry about the film plane¹², it is possible that thin films of anti-perovskites may also be topologically nontrivial. One may expect that both the inverted octet at Γ and the small avoided crossing at finite k can be tunable with

layer thickness. Moreover, given the wealth of phenomena in perovskite heterostructures and interfaces^{45–48}, it is likely that similarly diverse features can be found in the anti-perovskite counterparts. Likewise, applying strain serves as yet another experimental knob on these two gaps which will affect the topological class of the material³⁴. Finally, by applying pressure or tuning the chemical composition to interpolate between a trivial and a nontrivial (TCI) anti-perovskite, as done in the case of $\text{Pb}_{1-x}\text{Sn}_x\text{Se}$ ⁷, one may be able to observe a bulk gap closing and topological phase transition.

We conclude that the anti-perovskite family hosts a rich variety of features, now encompassing topology and symmetry. The existence of the Dirac octet at Γ undergoing band inversion leads to their classification as topological crystalline insulators endowed with robust metallic surface states. The presence of the high spin fermions fits naturally with the notion of TCIs, which allow for even number of band inversions unlike Z_2 topological insulators. The Dirac octet fermions are quite distinct from typical four-component Dirac or two-component Weyl fermions, and the topological phase diagram for the full $k \cdot p$ theory to quadratic order is expected to be quite rich. These new ingredients of topology, symmetry, and the high spin Dirac octet make the anti-perovskite family a promising playground for experimental and theoretical developments.

Acknowledgement: This work is supported by NSF Graduate Research Fellowship No. 0645960 (TH) and DOE Office of Basic Energy Sciences, Division of Materials Sciences and Engineering under award DE-SC0010526 (LF and JL).

* Electronic address: thsieh@mit.edu

† Electronic address: liujunweish@gmail.com

‡ Electronic address: liangfu@mit.edu

¹ L. Fu, Phys. Rev. Lett. **106**, 106802 (2011).

² M. Z. Hasan and C. L. Kane, Rev. Mod. Phys. **82**, 3045 (2010).

³ X. L. Qi and S. C. Zhang, Rev. Mod. Phys. **83**, 1057 (2011).

⁴ J. E. Moore, Nature **464**, 194 (2010).

⁵ T. Hsieh, H. Lin, J. Liu, W. Duan, A. Bansil, and L. Fu. Nat. Comm. **3**, 982 (2012).

⁶ Y. Tanaka, Z. Ren, T. Sato, K. Nakayama, S. Souma, T. Takahashi, K. Segawa, and Y. Ando. Nat. Phys. **8**, 800 (2012).

⁷ P. Dziawa, B. J. Kowalski, K. Dybko, R. Buczko, A. Szczerbakow, M. Szot, E. Lusakowska, T. Balasubramanian, B. M. Wojek, M. H. Berntsen, O. Tjernberg, and T. Story. Nat. Mat. **11**, 1023 (2012).

⁸ S.-Y. Xu, C. Liu, N. Alidoust, M. Neupane, D. Qian, I. Belopolski, J.D. Denlinger, Y.J. Wang, H. Lin, L.A. Wray, G. Landolt, B. Slomski, J.H. Dil, A. Marcinkova, E. Morosan, Q. Gibson, R. Sankar, F.C. Chou, R.J. Cava, A. Bansil, and M.Z. Hasan. Nat. Commun. **3**, 1192 (2012).

⁹ Y. Okada, M. Serbyn, H. Lin, D. Walkup, W. Zhou, C. Dhital, M. Neupane, S. Xu, Y.J. Wang, R. Sankar, F. Chou, A.

Bansil, M. Z. Hasan, S.D. Wilson, L. Fu, and V. Madhavan. Science, **341**, 1496 (2013).

¹⁰ M. Serbyn and L. Fu. Phys. Rev. B **90**, 035402 (2014)

¹¹ E. Tang and L. Fu. arXiv:1403.7523v1 (2014).

¹² J. Liu, T. H. Hsieh, P. Wei, W. Duan, J. Moodera, and L. Fu. Nat. Mat. **13**, 178 (2014).

¹³ M. Ezawa. Phys. Rev. B **89**, 195413 (2014).

¹⁴ C. Fang, M.J. Gilbert, and B.A. Bernevig. Phys. Rev. Lett. **112**, 046801 (2014).

¹⁵ F. Zhang, X. Li, J. Feng, C. L. Kane, and E. J. Mele. arXiv:1309.7682 (2013).

¹⁶ X. Qian, L. Fu and J. Li. arXiv:1403.3952 (2014).

¹⁷ R. Mong, A.M. Essin, and J.E. Moore. Phys. Rev. B **81**, 245209 (2010).

¹⁸ R. Takahashi and S. Murakami. Phys. Rev. Lett. **107**, 166805 (2011).

¹⁹ C. Fang, M.J. Gilbert, and B.A. Bernevig. Phys. Rev. Lett. **112**, 106401 (2014).

²⁰ P. Jadaun, D. Xiao, Q. Niu, and S.K. Banerjee. Phys. Rev. B **88**, 085110 (2013).

²¹ R.-J. Slager, A. Mesaros, V. Jurišić, and J. Zaanen. Nature Physics **9**, 98102 (2013).

²² W.A. Benalcazar, J.C.Y. Teo, and T.L. Hughes. Phys. Rev. B **89**, 224503 (2014).

- ²³ C-K Chiu, H. Yao, and S. Ryu. Phys. Rev. B **88**, 075142 (2013).
- ²⁴ C. X. Liu. arXiv:1304.6455 (2013).
- ²⁵ M. Kargarian and G.A. Fiete. Phys. Rev. Lett. **110**, 156403 (2013).
- ²⁶ M. Kindermann. arXiv:1309.1667 (2013).
- ²⁷ H. Weng, J. Zhao, Z. Wang, Z. Fang, and X. Dai. Phys. Rev. Lett. **112**, 016403 (2014).
- ²⁸ M. Ye, J. W. Allen, and K. Sun. arXiv:1307.7191 (2013).
- ²⁹ A. Widera and H. Schafer. Mater. Res. Bull. **15** 1805 (1980).
- ³⁰ T. He, Q. Huang, A. P. Ramirez, Y. Wang, K. A. Regan, N. Rogado, M. A. Hayward, M. K. Haas, J. S. Slusky, K. Inumara, H. W. Zandbergen, N. P. Ong, and R. J. Cava. Nature **411**, 54-56 (2001).
- ³¹ H. Tashiro. J. Kor. Phys. Soc. **63**, 3, 299-301 (2013)
- ³² K. Takenaka and H. Takagi. Appl. Phys. Lett. **87**, 261902 (2005)
- ³³ B. S. Wang, P. Tong, Y. P. Sun, X. B. Zhu, X. Luo, G. Li, W. H. Song, Z. R. Yang, and J. M. Dai J. Appl. Phys. **105**, 083907 (2009).
- ³⁴ Y. Sun, X-Q Chen, S. Yunoki, D. Li, and Y. Li Phys. Rev. Lett. **105**, 216406 (2010).
- ³⁵ T. Kariyado and M. Ogata. J. Phys. Soc. Jpn. **81** 064701 (2012).
- ³⁶ L. Fu and C.L. Kane, Phys. Rev. B **76**, 045302 (2007).
- ³⁷ J. C. Y. Teo, L. Fu and C. L. Kane, Phys. Rev. B **78**, 045426 (2007).
- ³⁸ Perdew, J. P., Burke, K. & Ernzerhof, M. Phys. Rev. Lett. **77** 3865-3868 (1996).
- ³⁹ P. E. Blöchl, Phys. Rev. B. **50**, 17953 (1994); G. Kresse and J. Joubert, Phys. Rev. B. **59**, 1758 (1999).
- ⁴⁰ G. Kress and J. Hafner, Phys. Rev. B. **48**, 13115 (1993); G. Kress and J. Furthmüller, Comput. Mater. Sci. **6**, 15 (1996); Phys. Rev. B. **54**, 11169 (1996).
- ⁴¹ A. V. Krukau, O. A. Vydrov, A. F. Izmaylov, and G. E. Scuseria, J. Chem. Phys. **125**, 224106 (2006)
- ⁴² Supplementary Material
- ⁴³ B.A. Bernevig, T.L. Hughes, and S-C. Zhang. Science **314**, 1757 (2006).
- ⁴⁴ T. Kariyado and M. Ogata. J. Phys. Soc. Jpn. **80** 083704 (2011).
- ⁴⁵ J. Chakhalian, A. J. Millis, and J. Rondinelli. Nature Materials **11**, 9294 (2012).
- ⁴⁶ D. Xiao, W. Zhu, Y. Ran, N. Nagaosa, and S. Okamoto. Nat. Comm. **2**:596 (2011).
- ⁴⁷ A. Ruegg, C. Mitra, A. A. Demkov, and G.A. Fiete. Phys. Rev. B **85**, 245131 (2012).
- ⁴⁸ D. Doennig, W.E. Pickett, and R. Pentcheva. Phys. Rev. B **89**, 121110(R) (2014).
- ⁴⁹ W.J. Elder, R.M. Ward, and J. Zhang. Phys. Rev. B **83**, 165210 (2011).
- ⁵⁰ J.M. Luttinger, Phys. Rev. **102**, 1030 (1956).
- ⁵¹ J. Vidal, X. Zhang, L. Yu, J.-W. Luo, and A. Zunger. Phys. Rev. B **84**, 041109(R) (2011).